Strain fields and line energies of dislocations in uranium dioxide

2010 J. Phys.: Condens. Matter 22 175004

(http://iopscience.iop.org/0953-8984/22/17/175004)

IOP Publishing Journal of Physics: Condensed Matter

J. Phys.: Condens. Matter **22** (2010) 175004 (8pp) doi:10.1088/0953-8984/22/17/175004

Strain fields and line energies of dislocations in uranium dioxide

David C Parfitt, Clare L Bishop, Mark R Wenman and Robin W Grimes

Department of Materials, Imperial College London, London SW7 2AZ, UK

Received 26 October 2009, in final form 7 March 2010
Published 7 April 2010
Online at stacks.iop.org/JPhysCM/22/175004

Abstract

Computer simulations are used to investigate the stability of typical dislocations in uranium dioxide. We explain in detail the methods used to produce the dislocation configurations and calculate the line energy and Peierls barrier for pure edge and screw dislocations with the shortest Burgers vector $\frac{1}{2}\langle 110\rangle$. The easiest slip system is found to be the $\{100\}\langle 110\rangle$ system for stoichiometric UO_2, in agreement with experimental observations. We also examine the different strain fields associated with these line defects and the close agreement between the strain field predicted by atomic scale models and the application of elastic theory. Molecular dynamics simulations are used to investigate the processes of slip that may occur for the three different edge dislocation geometries and nudged elastic band calculations are used to establish a value for the Peierls barrier, showing the possible utility of the method in investigating both thermodynamic average behaviour and dynamic processes such as creep and plastic deformation.

(Some figures in this article are in colour only in the electronic version)

1. Introduction

The structure and movement of dislocations in UO_2 is of significance both in determining the bulk properties of nuclear fuels, for example the creep rate [1–9], and also the clustering and mobility of defects on an atomic scale [10–13]. The influence of dislocation behaviour on nuclear fuel performance has also been recognized and explicitly incorporated into recent fuel performance codes [14, 15]. The behaviour of a dislocation is strongly linked with the behaviour of the dislocation core, which requires an understanding of the atomic scale interactions. Despite the growing application of modelling to better understand nuclear materials, there has been little work done on modelling dislocations in nuclear fuels. Conversely, the atomic scale modelling of effects such as radiation damage [16–22] or fission product behaviour [23–27] are well established. Therefore simple, robust atomic scale models of dislocations are of current interest.

We present here atomic scale simulations of a range of dislocations in UO_2 consisting of both edge and screw dislocations in a variety of orientations. We use both static energy minimization and dynamic simulation techniques to calculate the distribution of strain around the dislocation. We also calculate the line energy for each type of dislocation showing explicitly the contributions from the core region and the long range strain field, which agrees closely with established models of the extended dislocation structure from elastic theory. We calculate the energy of the Peierls barriers [28, 29], which is a measure of the ease of moving the dislocation core structure through the crystal via the process of slip, we present these results for the three different slip systems.

The intent here is to show that atomic scale simulations of dislocations in UO_2 are, with carefully constructed initial configurations, technically feasible using current simulation techniques. We also assess the stability and relative energies of four specific types of dislocation structure. Finally we comment upon the use of these techniques to examine the interaction of dislocations with isolated atomic defects.

2. Method

Crucial to any discussion of dislocations is the line energy, defined as the energy per unit length required to insert a dislocation into an otherwise pristine crystal lattice [30, 31]. Equally important is the displacement field, which is a vector field that relates each point in the perfect crystal to another point in the defective crystal. Both of these quantities are well defined in the macroscopic elastic limit, but can only

be calculated fully using atomic scale models to represent the dislocation core region. Using the line energy it is possible to assess the stability of the various types of dislocation configurations.

There are several ways of calculating the line energy of a given dislocation. For a theoretical approach, it is normal to consider general solutions of the displacement field that take into account the anisotropy of the crystal system. There are several numerical methods which relate the displacement field to the energy per atom via direct solution of the elastic constants matrix (see for example the work of Stroh [32–34] or Barnett and Swanger [35, 36]).

As we consider only straight, pure edge or screw dislocations with Burgers vectors along high symmetry directions within the crystal we choose an analytical approach where we calculate the line energy and displacement field from the elastic constants matrix. The line energy, $E(r)$, is given as an energy of the atoms within a cylinder of radius r,

$$E(r) = E_c + \frac{Kb^2}{4\pi} \ln\left(\frac{r}{r_c}\right) \quad (1)$$

where the Burgers vector of the dislocation is b, and expressions for K are derived below. E_c and r_c represent a partitioning of the dislocation into a core region (of radius r_c and energy E_c) that assumed not to behave according to the predictions of elastic theory. We also note that if explicit calculations of the displacements were not required then there are several articles that list modified Poisson's ratios in different crystal systems for common [37] and general rotations [38–40].

2.1. Pair potential model

Our calculations of dislocation line energies are based on static and dynamic atomic scale simulations employing a simple effective pair potential model for ion–ion interactions. The static simulations are used to calculate line energies and equilibrium strain fields. The dynamic simulations are used to demonstrate the thermal stability of the dislocations and their effectiveness in examining non-equilibrium processes such as slip and atomic scale migration.

There are many parameter sets that have been suggested for use in modelling UO_2 [41–43], here we employ a single potential set [43] that closely replicates the elastic properties of bulk UO_2. These will be important in correctly predicting the large scale behaviour of the dislocation in the elastic limit. Reviews of this potential and a comparison with other proposed sets have been published [44–46].

2.2. Construction of the dislocation configurations

The simulations are based upon dislocations that have been previously suggested as responsible for slip in UO_2 [47–49]. Specifically we considered slip in the ⟨110⟩ directions along {100}, {110} and {111} slip planes; we also consider a screw dislocation which we assume lies along the ⟨110⟩ directions such that the Burgers vector is minimized along a close packed plane. We show in table 1 the four different dislocation geometries along with the specific crystallographic planes and directions used in the construction of the simulation cells.

Table 1. Table showing the proposed slip systems and Burgers vectors considered here as well as the specific vectors used here. The line direction of the dislocation is taken to be along the z-axis and the Burgers vector is taken to along the y-axis (pure edge) and along the z-axis (pure screw).

Label	Type	Slip planes	Slip directions	Plane	Burgers vector	Line direction
(a)	Edge	{100}	⟨110⟩	(001)	$\frac{1}{2}$[110]	[$\bar{1}$10]
(b)	Edge	{110}	⟨110⟩	($\bar{1}$10)	$\frac{1}{2}$[110]	[001]
(c)	Edge	{111}	⟨110⟩	($\bar{1}$11)	$\frac{1}{2}$[110]	[1$\bar{1}$2]
(d)	Screw	{110}	⟨110⟩	—	$\frac{1}{2}$[110]	[110]

2.3. Initial atomic configuration

The calculation of the initial atomic configuration is complicated because the cell geometries (table 1) differ from the cubic case and therefore the line energies will (in the anisotropic case) depend not only upon the Burgers vector (which is the same in all the examples considered here) but also its alignment to the cubic axis of the UO_2 unit cell. This is a consequence of the anisotropic nature of the elastic constants matrix $\{c\}$, for the isotropic case (i.e. when $c_{44} = 2(c_{11} - c_{12})$, where c_{ij} are elements of the elastic constants matrix), there are more compact expressions that may be used [30].

We calculate the displacement and shear modulus K (equation (1)) via the following method.

(a) Calculation of the elements of the elastic constants matrix c_{ij} from numerical solution of the tensor linking the second derivative of energy with respect to the degrees of freedom of the crystal. The elastic constant matrix (and therefore values of K), are specific to the pair potentials used.

(b) Rotation of the elastic constants matrix, $\{c\}$ such that the new x, y and z components of the matrix point along the new cell axis in the sense that the Burgers vector lies along the y-axis (edge) or z-axis (screw) and the line of the dislocation points along the z-axis.

(c) There is no net strain parallel to the line of the dislocation, therefore we convert the elastic constants matrix to a reduced form $\{c'\}$ using the equation,

$$c'_{ij} = c_{ij} - \frac{c_{3j}c_{3i}}{c_{33}}. \quad (2)$$

(d) Several solutions exist to the general problem of calculating the displacement field [50–55]. We have employed the method advanced by Eshelby [50] and Foreman [51] where the line of the dislocation is taken along the z-axis and the solution proceeds via three simultaneous partial differential equations which are solved via complex variable analysis. In the appendix we quote the results obtained for the case of a pure edge dislocation and of a screw dislocation where the Burgers vector **b** is taken to lie along the y-axis (edge) or z-axis (screw) and we use the reduced elastic constants matrix $\{c'\}$.

For comparison with the elastic theory the shear modulus K from equation (1) is given from the elastic constants matrix by,

$$K = (c'_{11} - c'_{12})\left[\frac{c'_{66}(c'_{11} - c'_{12})}{(c'_{11} + c'_{12} + 2c'_{66})c'_{11}}\right] \quad (3)$$

for the case of an edge dislocation and,

$$K = (c'_{44}c'_{55} - c'^{2}_{45})^{\frac{1}{2}} \quad (4)$$

for a screw dislocation.

2.4. Simulation parameters

Having constructed the various initial defect configurations we now examine their properties using both static and molecular dynamics simulations. For the static simulations we used the code GULP version 3.4 [56–58], here the cell was constrained to be one-dimensional with the edges of the cell frozen in their initial configurations. For the molecular dynamics simulations we used the code DLPOLY [59, 60], with a vacuum gap of 1.5 nm separating the x and y directions of the cell, and the z-axis (along the dislocation line) was periodic. We are interested in the behaviour of the central dislocation region, to minimize any effect due to the vacuum gap or the interface between frozen atoms and relaxed atoms (although at long range these should be very similar) we chose large supercell sizes of ∼30 nm in the x- and y-directions and 4 nm in the z-direction, giving a total of around 300 000 atoms.

Each cell was equilibrated from its starting unrelaxed configuration at 300 K for a total of 5000 time steps (5 ps) to allow the core region of the dislocation to relax. The cell was then heated to 1200 K for another 5000 time steps to assess whether the dislocation configurations were thermally stable (at least on picosecond timescales), all those considered here remained intact. Following this, the cell was cooled to 10 K and the energy of the cell was minimized using a conjugate gradient procedure implemented within the DLPOLY code. A second reference cell that did not contain a dislocation, but otherwise contained the same number of ions was also simulated under the same conditions in order to provide a reference cell for calculating the line energies, though as discussed in section 3.1, this can be replaced with a calculation of the average lattice energy per formula unit. Molecular dynamics calculations of the slip were initiated from the end points of the 300 K simulations.

3. Results

Results are presented for each of the four dislocation geometries, examining the line energies, the calculated strain fields around the dislocations and for the edge dislocation cores the Peierls energy barrier.

3.1. Line energies of the dislocations

The line energy of a dislocation (equation (1)) increases logarithmically with the increasing radius of the region considered. To calculate the line energies from these simulations, we consider the total potential energy of a region of atoms within some cylinder whose central line coincides with the line of the dislocation core. The radius of this cylinder is effectively r in equation (1).

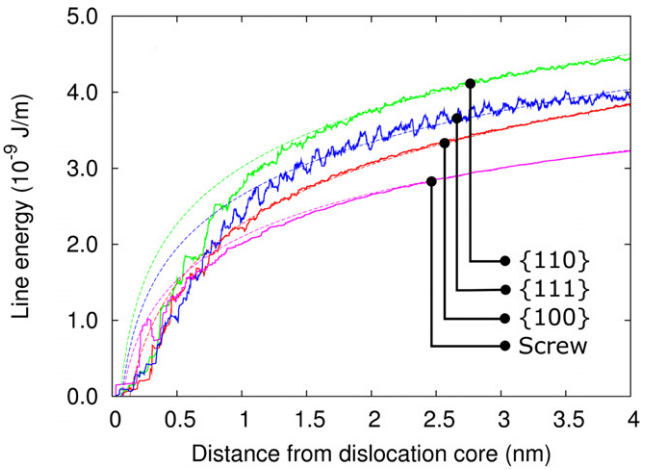

Figure 1. Plot of the line energies calculated from the simulations (solid lines) and compared with predicted values from elastic theory (equation (1)) shown as dotted lines for the four different cells.

The potential energy contained within this cylinder increases (to first order) as r^2, and so we need to subtract away the contributions due to the perfect (i.e. defect free) crystal to obtain the increase in potential energy that can be ascribed to the introduction of the dislocation. To do this we can subtract away the energy due to a similar sized cylinder of atoms in a cell without the dislocation or more succinctly calculate the average potential energy per U^{4+} and O^{2-} ion in a pure cell and subtract away this energy multiplied by the number of ions within the cylinder. The latter case assumes that

$$E(r) = E_{\mathrm{d}}(r) - E_{\mathrm{p}}(r) \simeq E_{\mathrm{d}} - \sum_{j=\mathrm{U,O}} N_j \langle E_j \rangle \quad (5)$$

where $E(r)$ is the energy due to the introduction of the dislocation measured at a distance r from the core, E_{d} and E_{p} are the energies contained within the cylinder with and without the dislocation respectively and N_j is the number of ions of type j each with average potential energy $\langle E_j \rangle$. We found that this approximation was well obeyed, serving as confirmation that our method of calculating the potential energy contained within the cylinders was accurate.

Figures 1(a)–(d) shows the line energy of a dislocation contained within a cylinder of radius r for the four different dislocation geometries considered here. We have fitted the core energy E_{c} from equation (1) to the simulation data defining (arbitrarily) the core radius r_{c} to be 3 nm and using the value of the shear modulus K calculated from equation (1) for each specific dislocation geometry. Table 2 shows the values of these parameters obtained from a fit to the data.

The agreement between simulations and the predictions of equation (1) for large values of r are excellent, particularly as the gradient of these lines are not fitted but are determined entirely by the values from equation (1). At low values of r there is significant deviation from linear elastic theory as we would expect in the core region.

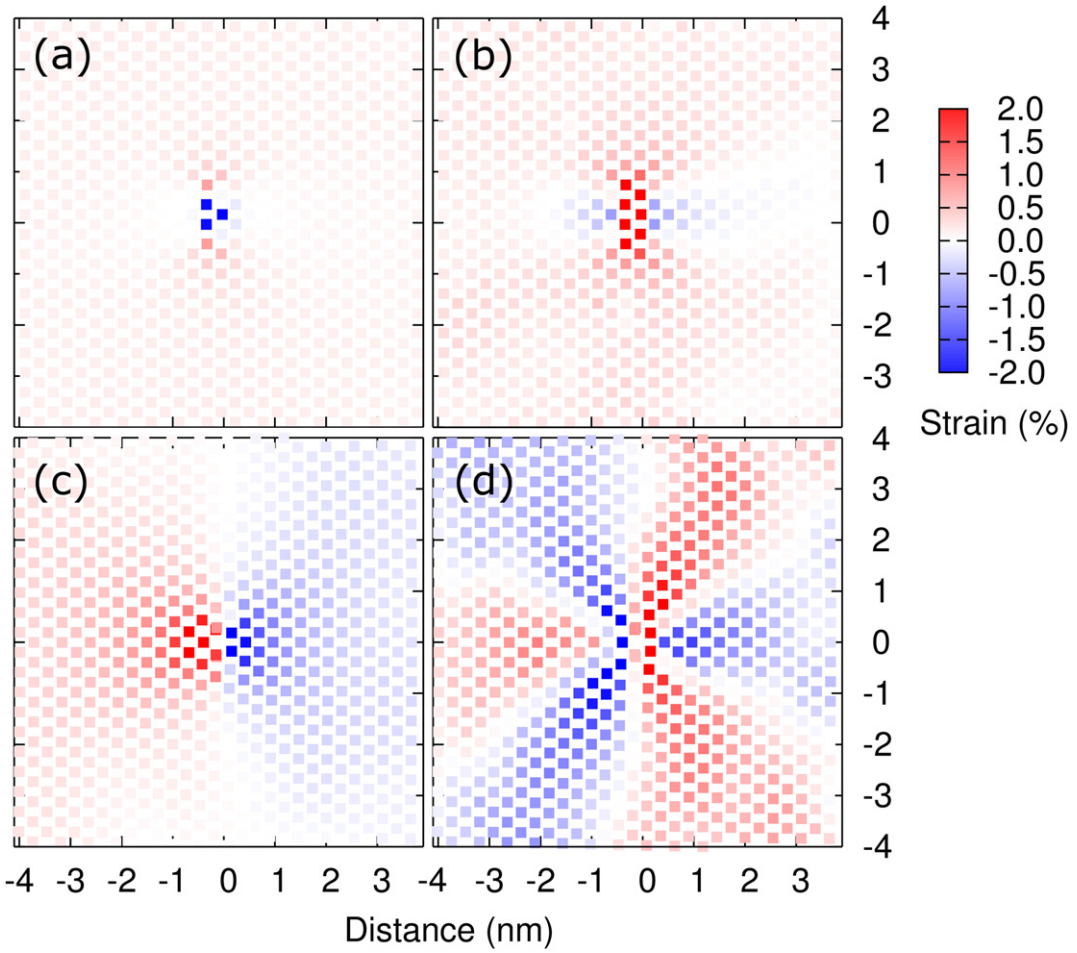

Figure 2. Typical strain field around dislocations with red colours showing tensile regions and blue showing compressive. Subplots show for a screw dislocation the (a) hydrostatic, i.e. the trace of the strain matrix, components and (b) the ϵ_{11} component, and similarly for the edge dislocation the (c) hydrostatic and (d) ϵ_{11} component.

Table 2. Table showing the fitted parameter of the core energy E_c, the core radius is fixed at 3 nm, equations are given in the text. The shear modulus term K calculated from equation (1) is also reported.

Cell	E_c (10^{-9} J m^{-1})	r_c (nm)	K (GPa)
{100} ⟨110⟩	3.51	3	95.6
{110} ⟨110⟩	4.19	3	90.9
{111} ⟨110⟩	3.75	3	85.1
Screw ⟨110⟩	3.00	3	69.8

The absolute values of line energies from figure 1 suggest that the most stable edge dislocation structures are the {100}⟨110⟩ system closely followed by the {111}⟨110⟩ system which has an energy ∼0.25 eV Å^{-1} greater. This agrees well with the prediction [49] that of the dominance of the {100}⟨110⟩ slip system in UO_2 with the {111}⟨110⟩ system existing as a secondary system.

3.2. Strain fields around the dislocation cores

We can also examine the strain field around the dislocation cores. To do this for each atom position in the simulation we take the positions of the surrounding U^{4+} ions from the energy minimized structure and calculate, using a least squares method, the matrix that best represents the linear transformation from the perfect crystal to the distorted cell with the dislocation. This assumes that the transformation is linear (i.e. that the nearest neighbourhood environment experience by each atom differs only from the perfect case by shear, stretch and rotational components). The elements of this matrix represent the strain components at each point surrounding the dislocation and the trace of this tensor then represents the hydrostatic strain.

Figure 2 illustrates four contour plots of the calculated strain for a (a) ⟨110⟩ screw dislocation showing the hydrostatic strain, (b) the same screw dislocation showing only the ϵ_{11} component of strain, (c) a {100}⟨110⟩ edge dislocation showing the hydrostatic strain, and (d) a {100}⟨110⟩ edge dislocation showing the ϵ_{11} component only. The strains surrounding the screw dislocation are small, only exceeding 1% for atoms very close to the dislocation core, where the concept of a linear relationship between perfect and distorted lattice has broken down. The hydrostatic strain around the screw dislocation is practically zero except for the three atoms immediately surrounding the core, this is in agreement with expectations [30, 31]. The strains surrounding the edge

dislocations are larger, and indeed the line energy of an edge dislocation is larger to accommodate this, and longer range. We also note the pair potential simulations reproduce the expected distribution of the components of the strain field ([30, page 77]) as well as the absolute hydrostatic strain.

The overall magnitude of the strains surrounding the dislocation cores is also interesting. We see firstly that the screw dislocations have much smaller hydrostatic strains surrounding them, whereas for the case of the edge dislocations the strain fields are much greater in magnitude, in a continuum model of course the screw dislocations have zero hydrostatic strain although the core relaxation here changes that slightly in our atomic scale models. The compressive and tensile regions will provide clustering points for atomic scale defects that have either large positive defect volumes (for example xenon atoms) or negative defect volumes (for example a neutral vacancy cluster); these may have important implications both for the mobility of dislocations (for example the formation of Cottrell atmospheres surrounding the cores [61]) or for the nucleation of bubbles of fission gases.

The close comparison between the predictions of elastic theory and those of the atomic scale simulations in the final displacements of the energy minimized dislocation structure. Far from the core region (beyond approximated 5 nm) the displacements are in good agreement: the difference between the original elastic theory positions and the atomic scale relaxed structure is less than 10 pm. Interestingly, however the displacements never quite go to zero, indicating that even in our large cells there is a small residual strain field cause by a core relaxation volume at the centre of the cell. Close to the core region there are significant differences between the initial configuration and the final relaxed structure.

3.3. Peierls barrier for edge dislocation slip

To quantify how easy it is to move a given dislocation we calculate the Peierls barrier [28, 29] for each of the three edge dislocation slip systems presented here. This is defined as the minimum energy barrier the atomic configuration must overcome to produce a second atomic configuration that is identical apart from a displacement of the dislocation core by a single lattice spacing. Due to the number of calculations required we used smaller cell sizes in these simulations. The cells were constructed as before but with linear dimensions of only 5 nm, with the periodic repeat unit (along the z-direction) around 2 nm depending upon the direction of the dislocation. These smaller cells considerably reduced the computational cost of the calculations at the expense of increasing the interaction with the fixed atoms at the boundary of the cell. However, in this case, the important quantity is the relative change in cell energy as the dislocation undergoes slip (and the interaction with the boundary region is approximately constant during this process). The transition energies calculated are therefore a good estimate of the values in large cells.

To calculate the Peierls barrier we implement two separate calculations, first using molecular dynamics to identify the reaction pathway and then a nudged elastic band calculation to calculate a value for the Peierls barrier. The molecular dynamics simulations use the dislocation configurations at 300 K for each of the three slip systems. A constant shear stress is applied to each of these cells such that the cell slowly distorts along a direction parallel to the Burgers vector, in the simulation the (frozen) atoms at the edges of the cell along the y-axis are translated at a speed of 1 m s^{-1} over the course of the simulation. This gives strain rates that are far higher than observed experimentally, but here we are interested in the response of a single dislocation over a time period of picoseconds. The application of this stress causes the dislocation to migrate along the $\langle 110 \rangle$ direction. Provided that the shear rate of the crystal is sufficiently slow, the dislocation will move in a series of single hops. Too rapid a shear rate and the dislocations move several lattice spacings in a single hop. Analysis of the atomic trajectories yields information about the intermediate state that occur between the hops.

Having induced slip processes for each of the dislocation geometries, we also now calculate a value for the Peierls barrier using a nudged elastic band calculation [62]. The initial and final states of this calculation require careful treatment. Although the starting configuration in each case contains the dislocation displaced by $\pm\frac{1}{4}\langle 110 \rangle$, the relaxation process was complex. The oxygen ions close to the dislocation core displayed a number of possible sites that were local energy minimum but not minima for the dislocation at a given position. In the molecular dynamics simulations we saw oxygen ions moving between all of these sites (the difference in energy was small, less than 0.1 eV) however we note that energy minimization of the molecular dynamics simulations does not always result in the lowest energy configuration. We examined several of these different configurations and chose ones that were the lowest in energy and also could be linked together to form a continuous migration process.

The transition pathway we identify using the examples from the molecular dynamics configurations. This is necessary as for a given migration, there are several ways of linking the two configurations by cleaving different set of bonds. We show an example in figure 3 where it is possible to link the initial and final states either by moving O^{2-} ions past each other or by cleaving a U–O bond (figure 3). In the first case the oxygen ions highlighted in the figure swap places; in the second case they do not. The success of the transition state search requires the correct pathway be chosen between the two.

Calculations of the minimum energy pathway use a nudged elastic band with 11 images equally spaced along the pathway. The initial set of images were constructed from a linear interpolation between initial and final states. We evaluated the energy and derivatives on each ion using the code GULP. To reduce the computational requirements, atoms a distance greater than 2.5 nm from the dislocation cores were held fixed (at their initial interpolated positions); atoms within this radius were moved according to the forces acting upon them due to the interatomic forces and the harmonic forces acting between adjacent images. The nudged elastic band algorithm was run until the absolute value of the out-of-plane force was less than the force tolerance of 5×10^{-4}.

Figure 4 shows the calculated minimum energy pathways for slip on the three proposed dislocation geometries. The

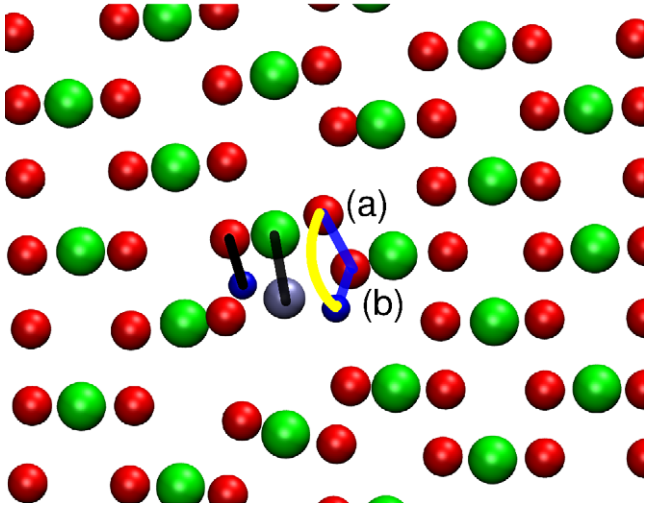

Figure 3. Possible pathways for slip in UO_2 on the {100}⟨110⟩ system. Oxygen ions are plotted as smaller red spheres, uranium ions as larger green spheres. Small blue spheres represent the position of the highlighted O–U–O triplet as the dislocation moves up the page. For slip to occur the oxygen ion labelled (a) must move to the highlighted position either directly (path indicated by the curved yellow line) or by exchanging places with ion (b) (path indicated by the straight blue lines). For the {100}⟨110⟩ slip system the calculated lowest energy pathway occurred via the direct (yellow) pathway.

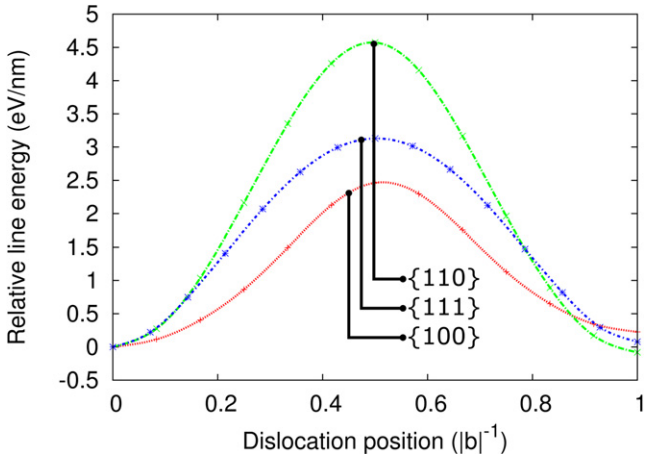

Figure 4. Migration barriers for the three different edge dislocation geometries, the energy is relative to the line energy at the equilibrium position. Crosses represent image positions across the Peierls barrier, lines are plotted as a guide to the eye.

lowest energy barrier occurs for the {100}⟨110⟩ system (2.5 eV nm^{-1}), with the {110}⟨110⟩ and {111}⟨110⟩ having higher barriers at 4.6 eV nm^{-1} and 3.1 eV nm^{-1}, respectively. The calculated values, showing the lowest Peierls barrier on the {100} slip plane, is in agreement with experiment [49] for the case of stoichiometric UO_2. Note also there is a small (<0.1 eV nm^{-1}) spread in the energies of the final configuration, this is due to the dislocation structure itself coming slightly closer to the edge of the simulation cell and therefore there being a slight change in the way the strain field is terminated.

4. Conclusions

The aims of this paper have been to describe the methods by which atomic scale simulations of dislocations can be performed in UO_2. We also examined the line energies and strain field surrounding four possible dislocation structures. Finally, we calculated the Peierls barrier for three possible slip systems.

The line energies and strain field surrounding the dislocations have been shown at large distances to be self-consistent with those expected from linear elastic theory. This gives confidence to the predictions made on the atomic scale behaviour of the core. It also means that modelling dislocations using a continuum model for distances further than around 3 nm appears to be compatible with atomic scale simulations. Recent developments in accurately calculating the electronic structure of UO_2 [23] using density functional theory may mean also that first principles calculations of the core structure (surrounded by an appropriate larger scale model) may also be permissible.

The Peierls barriers for slip along the {100}, {110} and {111} planes are in agreement with experimental evidence insofar as the lowest energy slip system is predicted to be the {100} system for stoichiometric UO_2. It is of interest to consider what influence of oxygen interstitials, oxygen vacancies and the possibility of U^{5+} formation may have upon the calculated energy barriers. The atomic scale description of these would of course require pair potentials (or electronic structure calculations) that could accurately describe each of these charged defects. In particular we note the easing of slip in the transition to hyper-stoichiometric UO_{2+x} and the switching between {100} and {110} [47–49]. A prediction of this behaviour would provide greater confidence in the values and techniques presented here.

Acknowledgments

This work was partly funded as part of the TSEC programme KNOO, and as such we are grateful to the EPSRC for funding under grant EP/C549465/1, and also supported by the European Commission through the FP7 F-BRIDGE project (Contract No. 211690). Calculations were performed on the Imperial College High Performance Computing Service. We would also like to thank Professor A H Heuer and Professor T E Mitchell for their helpful discussion and advice.

Appendix

Pure edge dislocation

Following Hirth and Lothe [30], we quote the displacement $(u_x, u_y, 0)$, applied to the crystal at a point (x, y). There are two distinct solutions to the complex variable problem, we first take the case that $2c'_{44} + c'_{12} - c'_{11} > 0$.

$$u_x = -\frac{b_y}{4\pi\lambda c'_{11}\sin 2\phi}\left[(c'_{11} - c'_{12})\cos\phi\ln(qt) - (c'_{11} + c'_{12})\sin\phi\tan^{-1}\left(\frac{x^2\sin 2\phi}{\lambda^2 y^2 - x^2\cos 2\phi}\right)\right] \quad (6)$$

$$u_y = -\frac{b_y}{4\pi}\left[\tan^{-1}\left(\frac{2xy\lambda\sin\phi}{x^2-\lambda^2y^2}\right) - \frac{c'^2_{11}-c'^2_{12}}{2c'_{11}c'_{66}\sin 2\phi}\ln\left(\frac{q}{t}\right)\right] \tag{7}$$

where,

$$q^2 = x^2 + 2xy\lambda\cos\phi + y^2\lambda^2 \tag{8}$$

$$t^2 = x^2 - 2xy\lambda\cos\phi + y^2\lambda^2 \tag{9}$$

$$\lambda = \left(\frac{c'_{11}}{c'_{22}}\right)^{\frac{1}{4}}. \tag{10}$$

And,

$$\cos 2\phi = \frac{c'^2_{12} + 2c'_{12}c'_{66} - c'^2_{11}}{2c'_{11}c'_{66}}. \tag{11}$$

For the case $2c'_{66} + c'_{12} - c'_{11} < 0$ the above equations produce an imaginary angle ϕ and we are required to use the secondary set of roots. In this case the equations for the displacement field are,

$$u_x = -\frac{b_y}{4\pi\lambda c'_{11}\sinh 2\delta}\Bigg[(c'_{11}-c'_{12})\sinh\delta\ln(qt) + \tfrac{1}{2}(c'_{11}+c'_{12})\cosh\delta \times \ln\left(\frac{\lambda^2y^2+x^2}{\lambda^2y^2+x^2(\cosh 2\delta+\sinh 2\delta)}\right)\Bigg] \tag{12}$$

$$u_y = -\frac{b_y}{4\pi}\left[\tan^{-1}\left(\frac{2xy\lambda\cosh\delta}{x^2-\lambda^2y^2}\right) - \frac{c'^2_{11}-c'^2_{12}}{2c'_{11}c'_{66}\sinh 2\delta}\tan^{-1}\left(\frac{2xy\lambda\sinh\delta}{x^2+\lambda^2y^2}\right)\right] \tag{13}$$

where $\phi = \pi/2 - \mathrm{i}\delta$, and δ is real and given by,

$$\cosh 2\delta = \frac{c'^2_{11} - c'^2_{12} - 2c'_{12}c'_{66}}{2c'_{11}c'_{66}}. \tag{14}$$

The product (qt) is, however, still real as q and t are redefined to be complex conjugates of each other,

$$q^2 = x^2 + y^2\lambda^2 + \mathrm{i}2xy\lambda\sinh\delta \tag{15}$$

$$t^2 = x^2 + y^2\lambda^2 - \mathrm{i}2xy\lambda\sinh\delta. \tag{16}$$

The value of λ (equation (10)) is unchanged.

Pure screw dislocation

Again following Hirth and Lothe [30], the displacements u_z are given in terms of the reduced elastic constants as,

$$u_z = -\frac{b}{2\pi}\tan^{-1}\frac{(c'_{44}c'_{55}-c'^2_{45})^{1/2}y}{c'_{44}x - c'_{45}y}. \tag{17}$$

References

[1] Desai T G, Millett P C and Wolf D 2008 *Acta Mater.* **56** 4489–97
[2] Na S H, Kim K H, Kim Y K, Kang K H and Ryu M J 2007 *Thermochim. Acta* **455** 109–13
[3] Knorr D B, Cannon R M and Coble R L 1989 *Acta Metall.* **37** 2103–23
[4] Gridnev A A, Dzalandinov D N, Zubarev P V and Panov A S 1985 *Sov. At. Energy* **59** 565–8
[5] Mohamed F A and Soliman M S 1982 *Mater. Sci. Eng.* **53** 185–90
[6] Chung T E and Davies T J 1979 *J. Nucl. Mater.* **79** 143–53
[7] Reynolds G L and Burton B 1979 *J. Nucl. Mater.* **82** 22–5
[8] Alamo A, Lefebvre J M and Soullard J 1978 *J. Nucl. Mater.* **75** 145–53
[9] Burton B and Reynolds G L 1974 *Phil. Mag.* **29** 1359–70
[10] Likhanskii V V, Sorokin A A and Khoruzhii O V 2004 *At. Energy* **96** 102–10
[11] Nogita K and Une K 1993 *J. Nucl. Sci. Technol.* **30** 900–10
[12] Van Uffelen P 2000 *J. Nucl. Mater.* **280** 275–84
[13] Jonnet J, Van Uffelen P, Wiss T, Staicu D, Remy B and Rest J 2008 *Nucl. Instrum. Methods Phys. Res.* B **266** 3008–12
[14] Veshchunov M S, Ozrin V D, Shestak V E, Tarasov V I, Dubourg R and Nicaise G 2006 *Nucl. Eng. Des.* **236** 179–200
[15] Veshchunov M S, Dubourg R, Ozrin V D, Shestak V E and Tarasov V I 2007 *J. Nucl. Mater.* **362** 327
[16] Van Brutzel L and Vincent-Aublant E 2008 *J. Nucl. Mater.* **377** 522–7
[17] Martin G, Maillard S, Van Brutzel L, Garcia P, Dorado B and Valot C 2009 *J. Nucl. Mater.* **385** 351
[18] Van Brutzel L and Vincent-Aublant E 2008 *J. Nucl. Mater.* **377** 522
[19] Van Brutzel L and Rarivomanantsoa M 2006 *J. Nucl. Mater.* **358** 209
[20] Van Brutzel L, Rarivomanantsoa M and Ghaleb D 2006 *J. Nucl. Mater.* **354** 28
[21] Parfitt D and Grimes R W 2008 *J. Nucl. Mater.* **381** 216
[22] Parfitt D and Grimes R W 2009 *J. Nucl. Mater.* **392** 28
[23] Dorado B, Amadon B, Freyss M and Bertolus M 2009 *Phys. Rev.* B **79** 235125
[24] Van Brutzel L, Chartier A and Crocombette J P 2008 *Phys. Rev.* B **78** 024111
[25] Busker G, Grimes R W and Bradford M R 2000 *J. Nucl. Mater.* **279** 46
[26] Grimes R W and Catlow C R A 1991 *Phil. Tran. R. Soc.* A **335** 609
[27] Grimes R W, Catlow C R A and Stoneham A M 1989 *J. Am. Ceram. Soc.* **72** 1856
[28] Peierls R E 1940 *Proc. Phys. Soc.* **52** 34
[29] Nabarro F R N 1947 *Proc. Phys. Soc.* **59** 256
[30] Hirth J P and Lothe J 1982 *Theory of Dislocations* (New York: Wiley)
[31] Hull D and Bacon D J 1984 *Introduction to Dislocations, Internation Series on Materials Science and Technology* (Oxford: Pergamon)
[32] Bacon D J, Barnett D M and Scattergood R O 1978 *Prog. Mater. Sci.* **23** 51
[33] Indembom V L, Alshits V I and Chernov V M 1980 *Defect in Crystals and their Computer Modeling* ed Yu A Ossipyan (Leningrad: Nauka) p 23
[34] Stroh A N 1962 *J. Math. Phys.* **41** 77
[35] Barnett D M and Swanger L A 1971 *Phys. Status Solidi* b **48** 419
[36] Barnett D M and Lothe J 1973 *Phys. Novegica* **7** 13
[37] Turley J and Sines G 1971 *J. Phys. D: Appl. Phys.* **4** 264

[38] Lieberman D S and Zirinsky S 1956 *Acta Crystallogr.* **9** 431
[39] Ballato A 1996 *IEEE Trans. Ultrason., Ferroelectr. Freq. Control* **43** 56
[40] Norris A N 2006 *Proc. R. Soc.* A **462** 3385
[41] Busker G, Chroneous A and Grimes R W 1999 *J. Am. Ceram. Soc.* **82** 1553
[42] Basak C B, Sengupta A K and Kamath H S 2003 *J. Alloys Compounds* **360** 210–6
[43] Morelon N D, Ghaleb D, Delaye J M and Van Brutzel L 2003 *Phil. Mag.* **83** 1533
[44] Govers K, Lemehov S, Hou M and Verwerft M 2007 *J. Nucl. Mater.* **366** 161
[45] Govers K, Lemehov S, Hou M and Verwerft M 2008 *J. Nucl. Mater.* **376** 66
[46] Devanathan R, Yu J and Weber W J 2009 *J. Chem. Phys.* **130** 174502
[47] Keller R J, Mitchell T E and Heuer A H 1981 *J. Physique* **42** 73
[48] Ashbee K H G and Yust C S 1982 *J. Nucl. Mater.* **110** 246
[49] Keller R J, Mitchell T E and Heuer A H 1988 *Acta Metall.* **36** 1073
[50] Eshelby J D, Read W T and Schockley W 1953 *Acta Metall.* **1** 251
[51] Foreman A J E 1955 *Acta Metall.* **3** 322
[52] Stroh A N 1958 *Phil. Mag.* **3** 625
[53] Spence G B 1962 *J. Appl. Phys.* **33** 729
[54] Chou Y T 1962 *J. Appl. Phys.* **33** 2747
[55] Seeger A and Schoeck G 1953 *Acta Metall.* **1** 519
[56] Gale J D 1997 *J. Faraday Trans.* **93** 629
[57] Gale J D 1996 *Phil. Mag.* **73** 3
[58] Gale J D and Rohl A L 2003 *Mol. Simul.* **29** 291
[59] Smith W 2006 *Mol. Simul.* **32** 933–1121
[60] Smith W and Todorov I T *The DLPOLY 3.0 User Manual* Daresbury Laboratory, United Kingdom
[61] Cottrell A H and Bilby B A 1947 *Proc. Phys. Soc.* **62** 49
[62] Henkelman G and Jonsson H 2000 *J. Chem. Phys.* **113** 9978